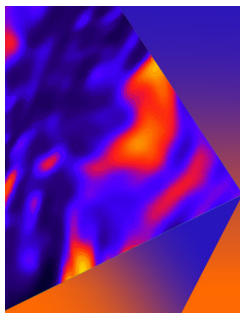# Tailoring MoS$_2$ domains size, doping, and light emission by the sulfurization temperature of ultra-thin MoO$_x$ films on sapphire

Salvatore Ethan Panasci ; Emanuela Schilirò ; Antal Koos ; Fabrizio Roccaforte ; Marco Cannas ; Simonpietro Agnello ; Béla Pécz ; Filippo Giannazzo ✉

Check for updates

View Online

Export Citation

Tailoring MoS$_2$ domains size, doping, and light emission by the sulfurization temperature of ultra-thin MoO$_x$ films on sapphire

View Online　　Export Citation　　CrossMark

Salvatore Ethan Panasci,[1] (iD) Emanuela Schilirò,[1] (iD) Antal Koos,[2] (iD) Fabrizio Roccaforte,[1] (iD) Marco Cannas,[3] (iD) Simonpietro Agnello,[3,4] (iD) Béla Pécz,[2] (iD) and Filippo Giannazzo[1,a] (iD)

AFFILIATIONS

[1]Consiglio Nazionale delle Ricerche-Istituto di Microelettronica e Microsistemi (CNR-IMM), Z.I. Strada VIII 5, 95121 Catania, Italy
[2]HUN-REN Centre for Energy Research, Institute of Technical Physics and Materials Science, Konkoly-Thege ut 29-33, 1121 Budapest, Hungary
[3]Department of Physics and Chemistry Emilio Segrè, University of Palermo, Via Archirafi 36, 90123 Palermo, Italy
[4]ATEN Center, University of Palermo, Viale delle Scienze Ed. 18, 90128 Palermo, Italy

[a]Author to whom correspondence should be addressed: filippo.giannazzo@imm.cnr.it

ABSTRACT

Thermal sulfurization of ultra-thin Mo-based films represents a promising approach for large-area growth of MoS$_2$. In this paper, we demonstrated that the crystalline quality (domains size and defects density), strain, doping, and light emission properties of monolayer (1L) MoS$_2$ obtained from sputter deposited MoO$_x$ films on a c-sapphire substrate can be tailored by the sulfurization temperature (T$_s$) in the range from 700 to 800 °C. Starting from a continuous film with a nanocrystalline domains structure at T$_s$ = 700 °C, a distribution of 1L MoS$_2$ triangular domains with 2.1 ± 0.6 and 2.6 ± 1.6 μm average sizes was obtained by increasing T$_s$ to 750 and 800 °C, respectively. The increase in T$_s$ was accompanied by a strong (25×) enhancement of the photoluminescence (PL) intensity. Furthermore, the average doping of MoS$_2$, evaluated from Raman analyses, evolved from a strong p-type doping ($\sim$1 × 10^{13} cm^{-2}) after T$_s$ = 700 °C, ascribed to residual MoO$_3$ in the film, to a low average n-type doping ($\sim$0.04 × 10^{13} cm^{-2}) after T$_s$ = 800 °C. The wide tunability of doping and PL of 1L MoS$_2$ by the sulfurization temperature can be exploited to tailor material properties for different specific applications.

Molybdenum disulfide (MoS$_2$) belongs to the family of transition metal dichalcogenides (TMDs), which are layered materials formed by stacks of X–M–X trilayers (being M = Mo, W transition metals and X = S, Se, and Te chalcogens) with covalent in-plane bonds and weak van der Waals interaction between the layers.[1] The bandgap tunability as a function of the number of layers is one of the most appealing features of TMDs. In particular, MoS$_2$ exhibits an indirect bandgap (1.2 eV) for bilayer to multilayer films, and a direct bandgap of 1.8–1.9 eV for a monolayer (1L).[2,3] This sizable energy bandgap, combined to good electron mobility values (up to $\sim$200 cm^2/V s),[4,5] makes MoS$_2$ a promising channel material for future ultra-thin body field effect transistors (FETs) beyond silicon.[6] In addition to electronics/optoelectronics,[7,8] MoS$_2$ has been explored in several other fields, including sensing,[9] photocatalysis,[10] and photovoltaics.[11] This wide application potential currently motivates the search of scalable

approaches to produce MoS$_2$ films with high control in terms of thickness uniformity, crystalline quality, doping, and photoluminescence (PL) properties.[12] To this purpose, both top-down and bottom-up methods have been explored, which exhibit advantages and drawbacks. Among top-down approaches, mechanical exfoliation from bulk crystals still provides the highest electronic quality MoS$_2$, despite the limited size and poor thickness control of produced MoS$_2$ flakes.[13,14] Recently, larger area (from mm^2 to cm^2) 1L MoS$_2$ membranes with excellent crystalline quality have been obtained by mechanical exfoliation from MoS$_2$ stamps on metal surfaces (particularly gold), followed by transfer to the final insulating substrates.[15,16] However, extending this method on wafer scale is currently not viable, especially due to the lack of MoS$_2$ bulk stamps of suitable size. Among bottom-up methods, chemical vapor deposition (CVD) is the most widely used and cost-effective approach for MoS$_2$ growth. To date, several variants of CVD

have been explored. The most common implementation is the vapor phase growth within a two-heating zone tube furnace, using S and MoO_3 powders as separate sources of the vapor precursors.[17] This method proved to be effective to obtain 1L MoS_2 flakes, typically with triangular shape and variable size (from ∼1 to ∼100 μm), on different substrates, including SiO_2,[17] sapphire,[18] SiC,[19,20] and GaN.[21,22] However, the difficulty to simultaneously control S and MoO_3 vapor fluxes on the target substrate[23,24] makes it challenging to achieve uniform MoS_2 coverage on wafer scale, whereas variations in the size, shape, and thickness of the flakes are typically observed in different wafer regions.[17,25] In this context, metal organic chemical vapor deposition (MOCVD) emerged in the last few years as the most advanced approach for wafer scale growth of MoS_2 (and other TMDs), thanks to the excellent control of the process parameters, such as the gas precursors fluxes within the reaction chamber.[26] The excellent uniformity and electronic/optoelectronic quality of MOCVD grown TMDs recently enabled impressive advancements in integrated electronics/optoelectronics, like the demonstration of active pixel arrays of MoS_2 phototransistors,[27] and 3D integration of up to three levels (tiers) of 2D field effect transistors.[28] Proper optimization of MOCVD also allowed direct deposition of MoS_2 at low temperature (<400 °C) for back-end-of-line applications.[29] Based on these progresses, it is expected that MOCVD will represent the method of choice for 3D monolithic integration of TMDs and the development of More-than-Moore applications. However, due to their complexity and high maintenance cost, MOCVD equipment remain not affordable for most academic laboratories and small enterprises. Hence, alternative approaches enabling wafer scale MoS_2 growth using commonly available equipment are still highly desirable. In this respect, a viable alternative to achieve uniform MoS_2 coverage on large area is the annealing under a S flux of Mo-based thin films pre-deposited on the substrate either by physical deposition (e.g., Mo or MoO_x sputtering or evaporation[30–32]) or by spin coating of liquid precursors [such as ammonium molybdate tetrahydrate $(NH_4)_6Mo_7O_{24}$[33]]. In this case, the uniformity of MoS_2 on large area is controlled by the initial Mo-based film coverage and thickness. As an example, uniform coating of SiC and GaN surfaces with 1L MoS_2 has been recently achieved by sulfurization at a temperature of 700 °C of sputter deposited ultra-thin (1–2 nm) MoO_x films.[34–36] The uniform 1L MoS_2 obtained under these sulfurization conditions was composed of domains with sizes from few tens to hundreds of nanometers, reminiscent of the nano-structure of the starting MoO_x film. Photoluminescence from these 1L MoS_2 films was significantly quenched, probably due to non-radiative excitonic recombination at domains boundaries. Furthermore, differently from the unintentional n-type doping typically observed in exfoliated or CVD grown MoS_2, these 1L-MoS_2 films showed a significant p-type doping explained by the presence of residual MoO_3 after the sulfurization process.[34,35] On the other hand, a discontinuous coating by micrometer-size triangular 1L MoS_2 domains with intense photoluminescence and a low average n-type doping has been recently reported by sulfurization at 800 °C of ultra-thin MoO_x films on c-sapphire substrates.[37] These results indicate the possibility of tailoring the structural, electronic, and optical emission properties of 1L MoS_2 by the sulfurization approach. However, a deeper understanding of the impact of relevant process parameters on the mechanisms of MoS_2 formation and the final crystalline quality, photoluminescence, and doping behavior is still required.

In this paper, optical and atomic force microscopy (AFM), combined with micro-Raman and micro-PL spectroscopy, have been employed to systematically investigate the role played by the sulfurization temperature T_s, in the range from 700 to 800 °C, on the morphological properties (coverage, domain size, and thickness), PL, and doping/strain of ultra-thin MoS_2 grown on sapphire. Starting from MoO_x films with identical initial thickness, we observed the evolution from a continuous nanocrystalline film, showing low photoluminescence and p-type doping (at $T_s = 700$ °C) to a distribution of single crystalline micrometer-size triangular 1L MoS_2 domains, showing prominent photoluminescence and n-type doping (at $T_s = 800$ °C). Based on these results, MoS_2 formation in this temperature range was explained by the interplay of different physical/chemical mechanisms, i.e., (i) the vapor–solid reaction between S and MoO_x, leading to the conversion of the starting MoO_x into a uniform nanocrystalline MoS_2 layer at $T_s = 700$ °C, and (ii) MoO_x evaporation/diffusion from/on sapphire surface, playing a crucial role in the growth of micrometer MoS_2 domains at $T_s = 750$ and 800 °C.

The starting MoO_x films on the c-sapphire substrates were obtained by DC magnetron sputtering from a Mo target using a Quorum Q300-TD Plus equipment, followed by natural oxidation in air. Samples with identical ∼1.8 nm thickness, evaluated by AFM step height measurement, were used for subsequent sulfurization experiments, carried out within a quartz tube with two different heating zones. The MoO_x/sapphire samples were placed in the central zone of the tube, heated at $T_s = 700$, 750, or 800 °C, whereas a crucible with sulfur powder was hosted in zone at a lower temperature of 150 °C. S vapors from the crucible were transported to the sample surface by a continuous Ar flux of 100 sccm for the entire duration of the process. The uniformity of MoS_2 coverage and the domains size were evaluated by optical microscopy and by AFM (operated in the tapping and peak-force tapping modes) using a Bruker Dimension Icon equipment with Si tips. Micro-PL spectra on the MoS_2 layers were acquired with a Horiba HR-Evolution system with a laser excitation wavelength of 532 nm (nominal maximum power 100 mW) in confocal configuration (100× objective). Furthermore, micro-Raman maps were collected using a WiTec Alpha equipment with a laser excitation at 532 nm, 1.5 mW power, and 100× objective.

The AFM morphology of the bare sapphire substrate and of the as-deposited MoO_x film are reported in Figs. S1(a) and S1(b) of the supplementary material. The c-sapphire surface is nearly atomically flat with a root mean square (RMS) roughness of 0.1 nm, while as-deposited MoO_x exhibits a nano-grains morphology, resulting in a higher RMS = 0.25 nm than the bare substrate. Figure 1 illustrates the evolution of MoS_2 coverage on sapphire surface, evaluated by optical microscopy and AFM, as a function of the sulfurization temperature. After MoO_x sulfurization at $T_s = 700$ °C, the presence of continuous MoS_2 film was deduced from the uniform optical contrast [see Fig. 1(a)]. This film also exhibits a nano-grains structure, as observed by the AFM image and the high resolution insert in Fig. 1(b). As compared to the morphology of as-deposited MoO_x, the formation of larger grains, resulting in an increased RMS = 0.35 nm, were observed after sulfurization at $T_s = 700$ °C, as illustrated in Fig. S1(c) of the supplementary material. To evaluate the size distribution of MoS_2 nano-grains, maps of the tip-surface adhesion force were acquired in the peak-force tapping mode. The adhesion force proved to be very sensitive in discriminating between the inner part of nano-domains and
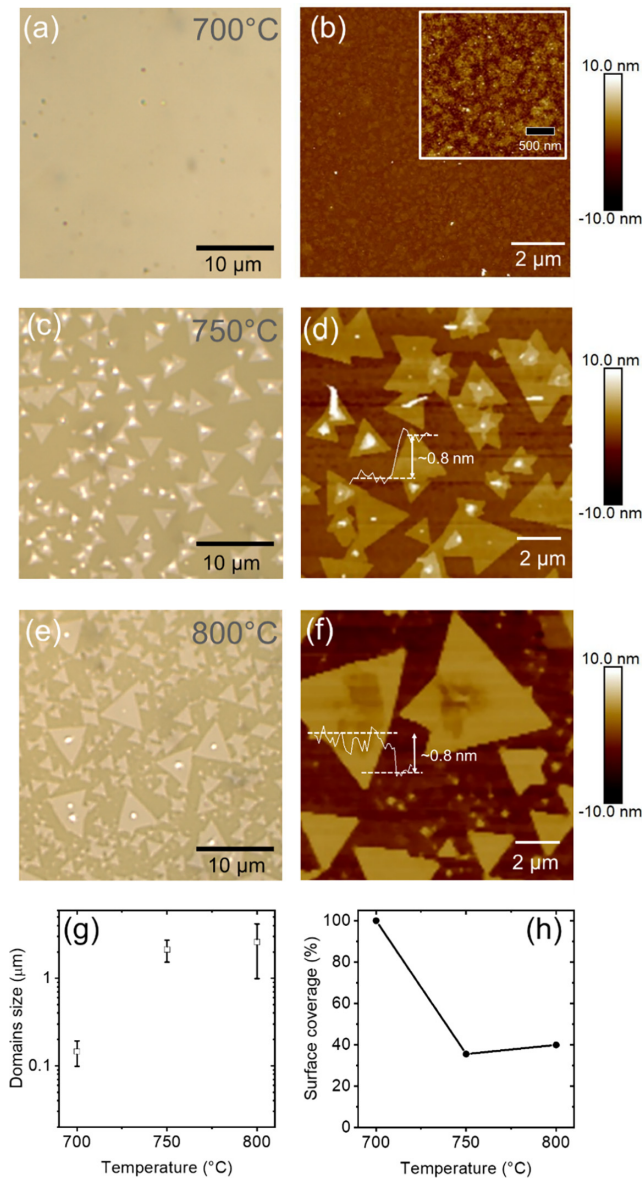
FIG. 1. Optical and morphological (AFM) images obtained for the MoS$_2$ on c-sapphire grown at 700 °C (a) and (b), 750 °C (c) and (d), and 800 °C (e) and (f). (g) Average MoS$_2$ domains size and (h) percentage of surface coverage on c-sapphire as a function of the sulfurization temperature.

their grain boundaries, as illustrated in Fig. S2(a) of the supplementary material. Figure S2(b) shows a histogram of lateral grains size distribution, obtained by statistical analysis on the adhesion force map, from which a MoS$_2$ domain size d = 150 ± 65 nm was evaluated. The continuous nanograin morphology of the film after sulfurization at 700 °C indicates a direct vapor–solid reaction between the incoming S and MoO$_x$ rules MoS$_2$ formation without a significant redistribution of Mo on the sapphire surface by diffusion processes. An average thickness of the MoS$_2$ film of ∼0.8 nm was evaluated by AFM step height measurements carried out on intentionally scratched regions of the film.

A very different morphology was observed by increasing the sulfurization temperature to T$_s$ = 750 °C, i.e., the partial coverage of sapphire surface by triangular MoS$_2$ domains with a nearly uniform size distributions and average dimension of 2.1 ± 0.6 μm [as deduced from the optical microscopy in Fig. 1(c)]. The domains exhibit mainly 1L thickness, evaluated by step height AFM analyses in Fig. 1(d), except for a multilayer region present at the center of some triangles. Finally, as illustrated in Figs. 1(e) and 1(f), the sulfurization process at T$_s$ = 800 °C results in a more inhomogeneous surface distribution of MoS$_2$ flakes, including both larger triangles (average size of 6.5 μm) and small ones (average size of 2 μm). The formation of these distributions of separated triangular domains indicates that the sulfurization processes at T$_s$ = 750 and 800 °C are accompanied by partial MoO$_x$ loss due to evaporation and a significant MoO$_x$ surface diffusion. Such a scenario is supported by micro-Raman analyses performed inside and outside triangular domains (see Fig. S5 of the supplementary material), from which a bare sapphire crystal without any intermediate MoS$_x$O$_y$ species in the region between MoS$_2$ domains can be also deduced.

Figures 1(g) and 1(h) summarize the changes in the MoS$_2$ domains size and the percentage of surface coverage as a function of T$_s$.

After this initial morphological analysis, the light emission properties of the MoS$_2$ layers produced at the different sulfurization temperatures were investigated by micro-photoluminescence (PL) spectroscopy. Figure 2(a) shows three representative PL spectra for MoS$_2$ grown at T$_s$ = 700 °C (black line), 750 °C (red line), and 800 °C (blue line). The sapphire second order Raman peak has been subtracted from all the spectra. Furthermore, they were normalized with respect to the respective MoS$_2$ Raman peaks in order to make them comparable in terms of intensity. Each spectrum exhibits a maximum intensity, associated with the neutral MoS$_2$ exciton peak A^0, and typical asymmetric shape, due to the convolution of two smaller components, i.e., the trion component at lower energy and the exciton component B at higher energy, respectively.[38] Noteworthy, the A^0 peak intensity showed a strong increase with increasing the sulfurization temperature. Specifically, starting from a quenched PL signal for the MoS$_2$ film grown at T$_s$ = 700 °C (multiplied by a factor of 5 to make it clearer), an enhancement of the peak's intensity by a factor of ∼10 was detected for MoS$_2$ domains grown at T$_s$ = 750 °C, and a further ∼2.5× increase was observed for domains grown at T$_s$ = 800 °C, as summarized in Fig. 2(b), left scale. Furthermore, the increase in peaks intensity is accompanied by a slight increase in the A^0 peak energy by ∼20 meV with increasing T$_s$ from 700 to 800 °C, as shown in Fig. 2(b), right scale. The observed differences in the light emission intensity represent strong evidence of the different crystalline quality of the MoS$_2$ samples. In fact, structural defects (including impurities or grain boundaries) are known to act as non-radiative recombination centers for excitons, causing a significant quenching of light emission from 1L MoS$_2$.[2,39]

In the following, a detailed micro-Raman spectroscopy investigation of the samples is reported to provide further insights on the thickness uniformity and crystalline quality of the MoS$_2$ films obtained at the different sulfurization temperatures. Figure 3(a) shows three representative Raman spectra collected after sulfurization at T$_s$ = 700 °C (bottom), 750 °C (middle), and 800 °C (top). The characteristic in-plane (E$_{2g}$) and out-of-plane (A$_{1g}$) first-order peaks of MoS$_2$ are clearly observed in the 370–420 cm^{-1} wavenumber range. The wavenumber difference ($\Delta\omega = \omega_{A1g} - \omega_{E2g}$) between these two main vibrational
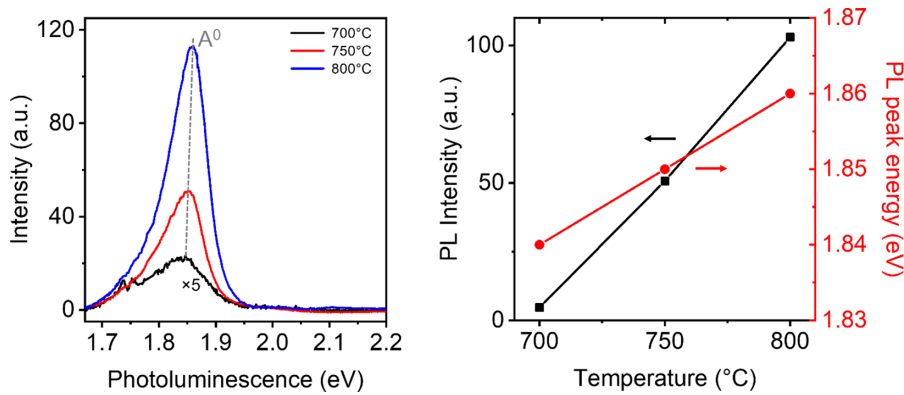
FIG. 2. (a) PL spectra for 1L-MoS$_2$ on c-sapphire at 700 °C (black line), 750 °C (red line), and 800 °C (blue line), where all the spectra are normalized with respect to the Raman MoS$_2$ peak. (b) Corresponding evolution of the PL exciton peak intensity and position as a function of the temperature, represented by black squares and red circles.
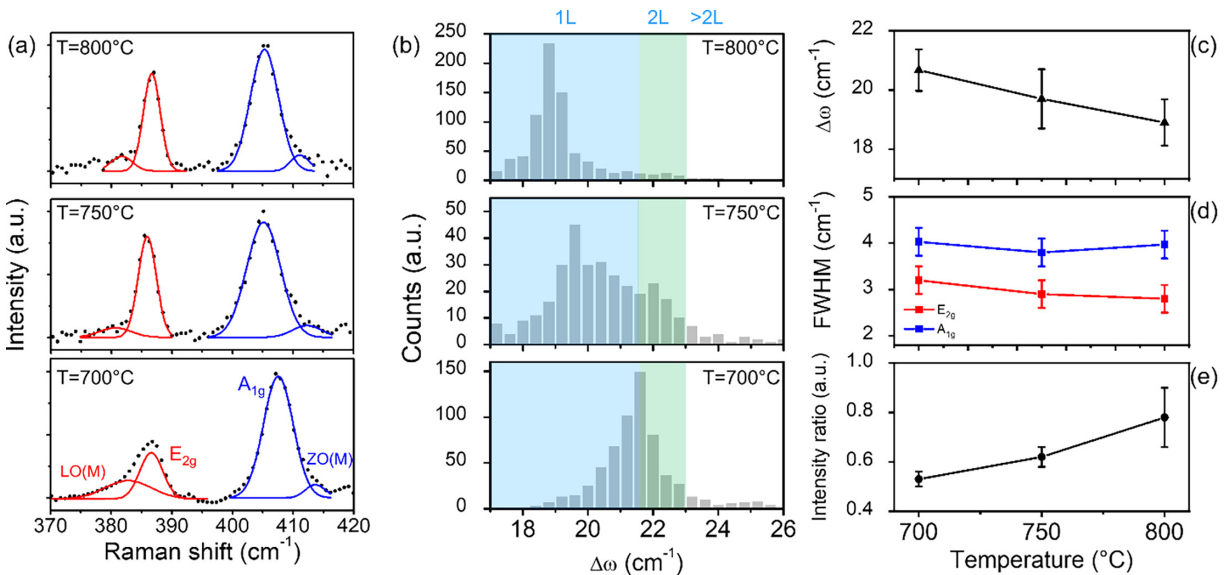
FIG. 3. (a) Raman spectra of MoS$_2$ grown on c-sapphire at 700 °C (bottom), 750 °C (middle), and 800 °C (top). (b) Histogram of the MoS$_2$ vibrational modes difference $\Delta\omega$ ($\omega_{A_{1g}} - \omega_{E_{2g}}$) distributions at 700 °C (bottom), 750 °C (middle), and 800 °C (top), where the blue, green, and white regions indicate the 1L, 2L, and multilayers MoS$_2$ ranges, respectively. Trend of (c) $\Delta\omega$, (d) FWHM, and (e) intensity ratio (E$_{2g}$/A$_{1g}$) as a function of the temperature.

peaks is commonly correlated with the number of layers in a MoS$_2$ film, with $\Delta\omega$ from ~18 to ~21.5 cm^{-1} corresponding to 1L and larger $\Delta\omega$ values associated with 2L and multilayers.[40] Figure 3(b) reports the histograms of $\Delta\omega$ values in the range between 18 and 26 cm^{-1}, obtained by performing a statistical analysis on a large number of Raman spectra collected on the three samples. After sulfurization at T$_s$ = 700 °C, the $\Delta\omega$ distribution was centered at 21.5 ± 1.2 cm^{-1}, indicating that the obtained MoS$_2$ film was mainly composed of 1L/2L with a small fraction corresponding to multilayers regions. Increasing the temperature to T$_s$ = 750 °C, the maximum of $\Delta\omega$ distribution undergoes a shift to a lower wavenumber value (19.7 cm^{-1}) associated with 1L MoS$_2$, while a multilayers contribution is still present, due to the thicker central region of some triangular domains [as shown by the optical and AFM images in Figs. 1(c) and 1(d)]. Finally, sulfurization at T$_s$ = 800 °C results in a narrow $\Delta\omega$

distribution centered at ~19 cm^{-1}, corresponding to 1L MoS$_2$, with negligible multilayer contributions. The shift of the maximum value of the $\Delta\omega$ distributions from ~21.5 to ~19 cm^{-1} with increasing T$_s$, as illustrated in Fig. 3(c), can be correlated with differences in the strain and doping of 1L MoS$_2$ membranes grown at the different temperatures[16,41,42] as discussed later on in this paper.

In addition to statistical information on the MoS$_2$ thickness uniformity, Raman analyses provided information on the crystalline quality of layers grown at the different sulfurization temperatures. The deconvolution analysis of the representative Raman spectra in Fig. 3(a) using Gaussian contributions allowed to identify, in addition to the E$_{2g}$ and A$_{1g}$ modes, two further components corresponding to the longitudinal [LO(M)] and out-of-plane optical modes [ZO(M)]. These vibrational modes, typically absent in the Raman spectra of a defect-free MoS$_2$, are activated by the presence of disorder or grain boundaries in
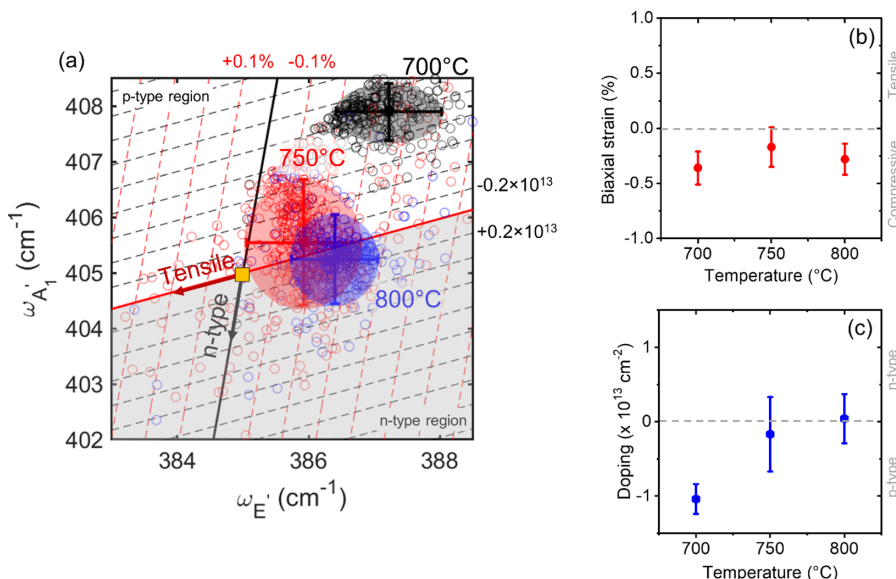
the MoS_2 crystalline structure, as explained by the phonon confinement model.[43,44] In particular, due to its nanocrystalline structure, the uniform MoS_2 film grown at $T_s = 700\,°C$ exhibits a significantly larger LO(M) contribution as compared to the micrometer-size single crystalline 1L MoS_2 domains obtained at higher T_s. On the other hand, the ZO(M) contribution was not particularly affected by the sulfurization temperature. In addition to the LO(M) and ZO(M) contributions, directly related to defects, the crystalline quality of 1L MoS_2 can be also evaluated by the FWHM and the intensity ratio of the two main vibrational modes E_{2g} and A_{1g}. These parameters were extracted by repeating the fitting procedure illustrated in Fig. 3(a) on the entire sets of Raman spectra for the three different samples. As summarized in Figs. 3(d) and 3(e), the FWHM of the E_{2g} and A_{1g} modes exhibits a decrease with increasing T_s,[45] whereas their intensity ratio (I_{E2g}/I_{A1g}) shows a significant increase.[45] Specifically, it was observed an I_{E2g}/I_{A1g} enhancement of ~68% when the MoS_2 was grown at 800 °C compared to that obtained at 700 °C. These aspects confirmed the higher MoS_2 crystalline quality obtained for $T_s > 700\,°C$.

As anticipated, the shift of the $\Delta\omega$ distributions maximum toward lower values with increasing T_s [as reported in Fig. 3(c)] can be ascribed to changes in the strain and doping of 1L MoS_2. In particular, the local values of the strain (ε) and doping (n) can be quantitatively extracted from micro-Raman spectra by a correlative plot of the A_{1g} vs E_{2g} peak positions.[16] Figure 4(a) shows such a correlative plot, where the black, red, and blue points are the experimental (ω_{E2g}, ω_{A1g}) peak positions for MoS_2 obtained by sulfurization at $T_s = 700$, 750, and 800 °C, respectively. The red and black straight lines represent the ideal ω_{E2g} vs ω_{A1g} behavior for a purely strained (strain line) and a purely doped (doping line) 1L MoS_2 membrane, respectively. The crossing point (ω^0_{A1g}, ω^0_{E2g}) of the strain and doping lines corresponds to the ideal case of unstrained and undoped MoS_2. Here, the Raman peaks positions for a suspended 1L-MoS_2 ($\omega^0_E = 385\,cm^{-1}$, $\omega^0_A = 405\,cm^{-1}$) have been taken as the best approximations for this ideal case.[46] Four regions with different doping type (p and n type) and strain (tensile and compressive) are separated in the (ω_{E2g}, ω_{A1g}) area by the

intersection of the strain and doping lines, and the specific doping values for each of the data point in Fig. 4(a) can be extracted by simple geometrical calculations.

By performing this analysis on all the data points, the average value and standard deviation of the biaxial strain (ε) and doping (n) for 1L MoS_2 grown at the different temperatures were evaluated, as reported in Figs. 4(b) and 4(c). Compressive strain values in the range between −0.2% and −0.3% were obtained for the three MoS_2 samples independently on the sulfurization temperature [Fig. 4(b)]. Differently, significant variations in the doping values and type were observed by increasing T_s, going from a high p-type doping of $(1.1 \pm 0.2) \times 10^{13}\,cm^{-2}$ for $T_s = 700\,°C$, to a smaller p-type doping of $(0.17 \pm 0.50) \times 10^{13}\,cm^{-2}$ for $T_s = 750\,°C$, until reaching a small n-type doping of $(0.04 \pm 0.33) \times 10^{13}\,cm^{-2}$ for $T_s = 800\,°C$, as shown in Fig. 4(c). The origin of the significant p-type doping in the MoS_2 sample obtained at the lowest sulfurization temperature can be ascribed to the presence of MoO_3 residues in the film, as demonstrated by XPS on samples grown under similar conditions.[34] In fact, MoO_3 is known to be a high work function oxide, leading to an overall Fermi level shift of MoS_2 to the valence band.[47] Thus, a reduction of MoO_3 residues in the MoS_2 domains obtained by sulfurization at higher temperature can explain the gradual reduction of the p-type doping and a transition to a low n-type average doping after $T_s = 800\,°C$.

In conclusion, we demonstrated that the crystalline quality (domains size and defects density), strain, doping, and light emission properties of monolayer (1L) MoS_2 obtained starting from sputter deposited MoO_x films on a c-sapphire substrate can be tailored by the sulfurization temperature (T_s) in the range from 700 to 800 °C. Starting from a continuous film with a nanocrystalline domains structure at $T_s = 700\,°C$, a distribution of 1L MoS_2 triangular domains with 2.1 ± 0.6 and $2.6 \pm 1.6\,\mu m$ average sizes was obtained by increasing T_s to 750 and 800 °C, respectively. Based on these results, MoS_2 formation in this temperature range was explained by the interplay of different physical/chemical mechanisms, i.e., (i) the vapor–solid reaction between S and MoO_x, leading to the conversion of the starting MoO_x

FIG. 4. (a) Correlative plot of the (ω_{E2g}, ω_{A1g}) Raman peak positions measured on MoS_2 obtained by sulfurization at $T_s = 700$ (black points), 750 (red points), and 800 °C (blue points). The red and black lines represent the ideal behavior for a purely strained and a purely doped 1L MoS_2 membrane, respectively, and their crossing point corresponds to the ideal case of unstrained and undoped MoS_2. (b) Biaxial strain as a function of the temperature, where the tensile and compressive contributions are separated by a gray dashed line. (c) Doping as a function of the temperature, where the n-type and p-type contributions are separated by a gray dashed line.

into a uniform nanocrystalline MoS_2 layer at $T_s = 700\,°C$, and (ii) MoO_x evaporation/diffusion from/on sapphire surface, playing a crucial role in the growth of micrometer MoS_2 domains at $T_s = 750$ and $800\,°C$. The evolution of morphology with T_S was accompanied by a strong ($25\times$) enhancement of the photoluminescence (PL) intensity, indicating a significant improvement of crystalline quality of the domains. Furthermore, the average doping of MoS_2, evaluated from Raman analyses, evolved from a strong p-type doping ($\sim 1 \times 10^{13}\,cm^{-2}$) at $T_s = 700\,°C$, ascribed to residual MoO_3 in the film, to a low average n-type doping ($\sim 0.04 \times 10^{13}\,cm^{-2}$) at $T_s = 800\,°C$. The wide tunability of doping and PL of 1L MoS_2 by the sulfurization temperature can be exploited to tailor material properties for different applications in electronics, optoelectronics, sensing, and catalysis. To this purpose, the main challenge for the scalability of this approach will be controlling the substrate temperature and sulfur flux on wafer scale, by designing of dedicated furnaces and adopting sulfur gas precursors instead of powders.

See the supplementary material for AFM morphology of sapphire, as-deposited MoO_x, and after sulfurization at $700\,°C$; tip-surface adhesion force map of MoS_2 grown at $700\,°C$ and histogram of nano-domains size distribution; maps of Raman peaks frequency difference $\Delta\omega = \omega_{A1g} - \omega_{E2g}$ for MoS_2 obtained at 700 and $800\,°C$; Raman signatures for MoO_xS_y reported in the literature; measured Raman spectra inside and outside MoS_2 triangular domains obtained by sulfurization at $800\,°C$.

AUTHOR DECLARATIONS
Conflict of Interest

The authors have no conflicts to disclose.

Author Contributions

Salvatore Ethan Panasci: Conceptualization (equal); Data curation (equal); Formal analysis (equal); Investigation (equal); Writing – original draft (equal). **Emanuela Schilirò:** Investigation (equal); Writing – review & editing (equal). **Antal Koos:** Formal analysis (equal); Investigation (equal); Writing – review & editing (equal). **Fabrizio Roccaforte:** Funding acquisition (equal); Project administration (equal); Writing – review & editing (equal). **Marco Cannas:** Methodology (equal); Writing – review & editing (equal). **Simonpietro Agnello:** Investigation (equal); Methodology (equal);

Writing – review & editing (equal). **Béla Pécz:** Funding acquisition (equal); Investigation (equal); Project administration (equal); Writing – review & editing (equal). **Filippo Giannazzo:** Conceptualization (lead); Funding acquisition (lead); Methodology (equal); Project administration (lead); Supervision (equal); Writing – review & editing (lead).

DATA AVAILABILITY

The data that support the findings of this study are available from the corresponding author upon reasonable request.

REFERENCES

[1] A. K. Geim and I. V. Grigorieva, "Van der Waals heterostructures," Nature **499**, 419–425 (2013).

[2] A. Splendiani, L. Sun, Y. Zhang, T. Li, J. Kim, C. Y. Chim, G. Galli, and F. Wang, "Emerging photoluminescence in monolayer MoS_2," Nano Lett. **10**, 1271–1275 (2010).

[3] K. F. Mak, C. Lee, J. Hone, J. Shan, and T. F. Heinz, "Atomically thin MoS_2: A new direct-gap semiconductor," Phys. Rev. Lett. **105**, 136805 (2010).

[4] B. Radisavljevic, A. Radenovic, J. Brivio, V. Giacometti, and A. Kis, "Single-layer MoS_2 transistors," Nat. Nanotechnol. **6**, 147–150 (2011).

[5] B. Radisavljevic and A. Kis, "Mobility engineering and a metal–insulator transition in monolayer MoS_2," Nat. Mater. **12**(9), 815–820 (2013).

[6] B. Radisavljevic, M. B. Whitwick, and A. Kis, "Integrated circuits and logic operations based on single-layer MoS_2," ACS Nano **5**, 9934–9938 (2011).

[7] Q. H. Wang, K. Kalantar-Zadeh, A. Kis, J. N. Coleman, and M. S. Strano, "Electronics and optoelectronics of two-dimensional transition metal dichalcogenides," Nat. Nanotechnol. **7**, 699–712 (2012).

[8] E. Singh, P. Singh, K. S. Kim, G. Y. Yeom, and H. S. Nalwa, "Flexible molybdenum disulfide (MoS_2) atomic layers for wearable electronics and optoelectronics," ACS Appl. Mater. Interfaces **11**, 11061–11105 (2019).

[9] F. K. Perkins, A. L. Friedman, E. Cobas, P. M. Campbell, G. G. Jernigan, and B. T. Jonker, "Chemical vapor sensing with monolayer MoS_2," Nano Lett. **13**(2), 668–673 (2013).

[10] E. Parzinger, B. Miller, B. Blaschke, J. A. Garrido, J. W. Ager, A. Holleitner, and U. Wurstbauer, "Photocatalytic stability of single-and few-layer MoS_2," ACS Nano **9**, 11302–11309 (2015).

[11] O. Lopez-Sanchez, E. Alarcon Llado, V. Koman, A. Fontcuberta i Morral, A. Radenovic, and A. Kis, "Light generation and harvesting in a van der Waals heterostructure," Acs Nano **8**, 3042–3048 (2014).

[12] S. Najmaei, J. Yuan, J. Zhang, P. Ajayan, and J. Lou, "Synthesis and defect investigation of two-dimensional molybdenum disulfide atomic layers," Acc. Chem. Res. **48**, 31–40 (2015).

[13] K. S. Novoselov, D. Jiang, F. Schedin, T. J. Booth, V. V. Khotkevich, S. V. Morozov, and A. K. Geim, "Two-dimensional atomic crystals," Proc. Natl. Acad. Sci. U. S. A. **102**, 10451–10453 (2005).

[14] H. Li, J. Wu, Z. Yin, and H. Zhang, "Preparation and applications of mechanically exfoliated single-layer and multilayer MoS_2 and WSe_2 nanosheets," Acc. Chem. Res. **47**(4), 1067–1075 (2014).

[15] L. Pirker, J. Honolka, M. Velicky, and O. Frank, "When 2D materials meet metals," 2D Mater. **11**, 022003 (2024).

[16] S. E. Panasci, E. Schilirò, G. Greco, M. Cannas, F. M. Gelardi, S. Agnello, F. Roccaforte, and F. Giannazzo, "Strain, doping and electronic transport of large area monolater MoS_2 exfoliated on gold and transferred to an insulating substrate," ACS Appl. Mater. Interfaces **13**, 31248–31259 (2021).

[17] Y. H. Lee, X. Q. Zhang, W. Zhang, M. T. Chang, C. T. Lin, K. D. Chang, Y. C. Yu, J. T. W. Wang, C. S. Chang, L. J. Li, and T. S. Lin, "Synthesis of large-area MoS_2 atomic layers with chemical vapor deposition," Adv. Mater. **24**, 2320–2325 (2012).

[18] D. Dumcenco, D. Ovchinnikov, K. Marinov, P. Lazic, M. Gibertini, N. Marzari, O. L. Sanchez, Y. C. Kung, D. Krasnozhon, M. W. Chen, S. Bertolazzi, P. Gillet, A. F. i Morral, A. Radenovic, and A. Kis, "Large-area epitaxial monolayer MoS_2," ACS Nano **9**, 4611–4620 (2015).

[19]E. W. Lee II, L. Ma, D. N. Nath, C. H. Lee, A. Arehart, Y. Wu, and S. Rajan, "Growth and electrical characterization of two-dimensional layered MoS$_2$/SiC heterojunctions," Appl. Phys. Lett. **105**, 203504 (2014).

[20]S. E. Panasci, I. Deretzis, E. Schilirò, A. La Magna, F. Roccaforte, A. Koos, B. Pécz, S. Agnello, M. Cannas, and F. Giannazzo, "Interface structure and doping of chemical vapor deposition-grown MoS$_2$ on 4H–SiC by microscopic analyses and ab initio calculations," Phys. Stat. Sol. RRL **17**, 2300218 (2023).

[21]D. Ruzmetov, K. Zhang, G. Stan, B. Kalanyan, G. Bhimanapati, S. M. Eichfeld, R. A. Burke, P. B. Shah, T. P. O'Regan, F. J. Crowne, A. G. Birdwell, J. A. Robinson, A. V. Davydov, and T. G. Ivanov, "Vertical 2D/3D semiconductor heterostructures based on epitaxial molybdenum disulfide and gallium nitride," ACS Nano **10**, 3580–3588 (2016).

[22]S. E. Panasci, I. Deretzis, E. Schilirò, A. La Magna, F. Roccaforte, A. Koos, M. Nemeth, B. Pécz, M. Cannas, S. Agnello, and F. Giannazzo, "Interface properties of MoS$_2$ van der Waals heterojunctions with GaN," Nanomaterials **14**, 133 (2024).

[23]S. Wang, Y. Rong, Y. Fan, M. Pacios, H. Bhaskaran, K. He, and J. H. Warner, "Shape evolution of monolayer MoS$_2$ crystals grown by chemical vapor deposition," Chem. Mater. **26**, 6371–6379 (2014).

[24]S. Y. Yang, G. W. Shim, S. B. Seo, and S. Y. Choi, "Effective shape-controlled growth of monolayer MoS$_2$ flakes by powder based chemical vapor deposition," Nano Res. **10**, 255–262 (2017).

[25]J. Jeon, S. K. Jang, S. M. Jeon, G. Yoo, Y. H. Jang, J. H. Park, and S. Lee, "Layer-controlled CVD growth of large-area two-dimensional MoS$_2$ films," Nanoscale **7**, 1688–1695 (2015).

[26]K. Kang, S. Xie, L. Huang, Y. Han, P. Y. Huang, K. F. Mak, C.-J. Kim, D. Muller, and J. Park, "High-mobility three-atom-thick semiconducting films with wafer-scale homogeneity," Nature **520**, 656–660 (2015).

[27]A. Dodda, D. Jayachandran, A. Pannone, N. Trainor, S. P. Stepanoff, M. A. Steves, S. S. Radhakrishnan, S. Bachu, C. W. Ordonez, J. R. Shallenberger, J. M. Redwing, K. L. Knappenberger, D. E. Wolfe, and S. Das, "Active pixel sensor matrix based on monolayer MoS$_2$ phototransistor array," Nat. Mater. **21**, 1379–1387 (2022).

[28]D. Jayachandran, R. Pendurthi, M. U. Karim Sadaf, N. U. Sakib, A. Pannone, C. Chen, Y. Han, N. Trainor, S. Kumari, T. V. Mc Knight, J. M. Redwing, Y. Yang, and S. Das, "Three dimensional integration of two dimensional field effect transistors," Nature **625**, 276–281 (2024).

[29]J. Zhu, J. H. Park, S. A. Vitale, W. Ge, G. S. Jung, J. Wang, M. Mohamed, T. Zhang, M. Ashok, M. Xue, X. Zheng, Z. Wang, J. Hansryd, A. P. Chandrakasan, J. Kong, and T. Palacios, "Low-thermal-budget synthesis of monolayer molybdenum disulfide for silicon back-end-of-line integration on a 200 mm platform," Nat. Nanotechnol. **18**, 456–463 (2023).

[30]Y. C. Lin, W. Zhang, J. K. Huang, K. K. Liu, Y. H. Lee, C. T. Liang, C. W. Chu, and L. J. Li, "Wafer-scale MoS$_2$ thin layers prepared by MoO$_3$ sulfurization," Nanoscale **4**, 6637–6641 (2012).

[31]S. E. Panasci, A. Koos, E. Schilirò, S. Di Franco, G. Greco, P. Fiorenza, F. Roccaforte, S. Agnello, M. Cannas, F. M. Gelardi, A. Sulyok, M. Nemeth, B. Pécz, and F. Giannazzo, "Multiscale investigation of the structural, electrical and photoluminescence properties of MoS$_2$ obtained by MoO$_3$ sulfurization," Nanomaterials **12**, 182 (2022).

[32]S. Vangelista, E. Cinquanta, C. Martella, M. Alia, M. Longo, A. Lamperti, R. Mantovan, F. B. Basset, F. Pezzoli, and A. Molle, "Towards a uniform and large-scale deposition of MoS$_2$ nanosheets via sulfurization of ultra-thin Mo-based solid films," Nanotechnology **27**, 175703 (2016).

[33]F. Esposito, M. Bosi, G. Attolini, F. Rossi, S. E. Panasci, P. Fiorenza, F. Giannazzo, F. Fabbri, and L. Seravalli, "Role of density gradients in the growth dynamics of 2-dimensional MoS$_2$ using liquid phase molybdenum precursor in chemical vapor deposition," Appl. Surf. Sci. **639**, 158230 (2023).

[34]F. Giannazzo, S. E. Panasci, E. Schilirò, F. Roccaforte, A. Koos, M. Nemeth, and B. Pécz, "Esaki diode behavior in highly uniform MoS$_2$/silicon carbide heterojunctions," Adv. Mater. Interfaces **9**, 2200915 (2022).

[35]F. Giannazzo, S. E. Panasci, E. Schilirò, G. Greco, F. Roccaforte, G. Sfuncia, G. Nicotra, M. Cannas, S. Agnello, E. Frayssinet, Y. Cordier, A. Michon, A. Koos, and B. Pécz, "Atomic resolution interface structure and vertical current injection in highly uniform MoS$_2$ heterojunctions with bulk GaN," Appl. Surf. Sci **631**, 157513 (2023).

[36]F. Giannazzo, S. E. Panasci, E. Schilirò, A. Koos, and B. Pécz, "Integration of graphene and MoS$_2$ on silicon carbide: Materials science challenges and novel devices," Mater. Sci. Semicond. Process. **174**, 108220 (2024).

[37]S. E. Panasci, E. Schilirò, A. Koos, M. Nemeth, M. Cannas, S. Agnello, F. Roccaforte, B. Pécz, and F. Giannazzo, "Micrometer-size crystalline monolayer MoS$_2$ domains obtained by sulfurization of molybdenum oxide ultrathin films," Microelectron. Eng. **274**, 111967 (2023).

[38]S. E. Panasci, E. Schilirò, F. Migliore, M. Cannas, F. M. Gelardi, F. Roccaforte, F. Giannazzo, and S. Agnello, "Substrate impact on the thickness dependence of vibrational and optical properties of large area MoS$_2$ produced by gold-assisted exfoliation," Appl. Phys. Lett. **119**, 093103 (2021).

[39]A. Zafar, H. Nan, Z. Zafar, Z. Wu, J. Jiang, Y. You, and Z. Ni, "Probing the intrinsic optical quality of CVD grown MoS$_2$," Nano Res. **10**, 1608–1617 (2017).

[40]C. Lee, H. Yan, L. E. Brus, T. F. Heinz, J. Hone, and S. Ryu, "Anomalous lattice vibrations of single-and few-layer MoS$_2$," ACS Nano **4**, 2695–2700 (2010).

[41]A. Michail, N. Delikoukos, J. Parthenios, C. Galiotis, and K. Papagelis, "Optical detection of strain and doping inhomogeneities in single layer MoS$_2$," Appl. Phys. Lett. **108**, 173102 (2016).

[42]J. E. Lee, G. Ahn, J. Shim, Y. S. Lee, and S. Ryu, "Optical separation of mechanical strain from charge doping in graphene," Nat. Commun. **3**, 1024 (2012).

[43]E. M. Ferreira, M. V. Moutinho, F. Stavale, M. M. Lucchese, R. B. Capaz, C. A. Achete, and A. Jorio, "Evolution of the Raman spectra from single-, few-, and many-layer graphene with increasing disorder," Phys. Rev. B **82**, 125429 (2010).

[44]S. Mignuzzi, A. J. Pollard, N. Bonini, B. Brennan, I. S. Gilmore, M. A. Pimenta, D. Richards, and D. Roy, "Effect of disorder on Raman scattering of single-layer MoS$_2$," Phys. Rev. B **91**, 195411 (2015).

[45]C. R. Wu, X. R. Chang, C. H. Wu, and S. Y. Lin, "The growth mechanism of transition metal dichalcogenides by using sulfurization of pre-deposited transition metals and the 2D crystal hetero-structure establishment," Sci. Rep. **7**, 42146 (2017).

[46]D. Lloyd, X. Liu, J. W. Christopher, L. Cantley, A. Wadehra, B. L. Kim, B. B. Goldberg, A. K. Swan, and J. S. Bunch, "Band gap engineering with ultralarge biaxial strains in suspended monolayer MoS$_2$," Nano Lett. **16**, 5836–5841 (2016).

[47]F. Giannazzo, G. Fisichella, G. Greco, S. Di Franco, I. Deretzis, A. La Magna, C. Bongiorno, G. Nicotra, C. Spinella, M. Scopelliti, B. Pignataro, S. Agnello, and F. Roccaforte, "Ambipolar MoS$_2$ transistors by nanoscale tailoring of schottky barrier using oxygen plasma functionalization," ACS Appl. Mater. Interfaces **9**, 23164 (2017).

03 July 2024 04:33:33